EFFECT OF SURFACE DEAD-LAYER QUENCHING ON THE THIRD-ORDER NONLINEAR OPTICAL PROPERTIES OF NANOPARTICLES

Koraboev Kamoliddin Abdushukurovich – *assistant teacher*
qkamoliddin956@gmail.com
University of Geological Sciences

NANOZARRAChALARNING UChUNChI TARTIBLI NOChIZIQLI OPTIK XUSUSIYATLARIGA "SIRT QATLAM" SO'NDIRISh HODISASINING TA'SIRI

Qoraboyev Kamoliddin Abdishukurovich – *assistent o'qituvchi*
Geologiya fanlari universiteti

ВЛИЯНИЕ ЭФФЕКТА ГАШЕНИЯ ПОВЕРХНОСТНЫМ «МЁРТВЫМ СЛОЕМ» НА НЕЛИНЕЙНО-ОПТИЧЕСКИЕ СВОЙСТВА ТРЕТЬЕГО ПОРЯДКА НАНОЧАСТИЦ

Корабоев Камолиддин Абдишукурович – *ассистент преподаватель*
Университет геологических наук

Tayanch so'zlar: vodorodsimon yaqinlashuv, eksiton energiyasi, uchinchi tartibli nochiziqli optik kirituvchanlik, CdSe kvant nuqtalari, kaskadli virtual o'tishlar, sirt o'lik qatlami, kvant chegaralanish.

Rezyume. CdSe kvant nuqtalarining uchinchi tartibli nochiziqli optik kirituvchanligi $(\chi^{(3)})$ bo'yicha nazariya (R kamayishi bilan monoton o'sish) va tajriba $R < 2\ nm$ da keskin so'nish) o'rtasidagi tafovutni bartaraf etish uchun Boyd, Brus modellari va sirt "o'lik qatlami" korreksiyasini birlashtiruvchi analitik model taklif etiladi. Model $\chi^{(3)}(R)$ning monoton bo'lmagan bog'liqligini va optimal radiusni $R_{opt} \approx 2.5$ nm bashorat qiladi; hisoblangan qiymatlar $(10^{-20} - 10^{-22}\ \text{m}^2/\text{V}^2)$ CdSe/ZnS-MOF nazariy bahosi va CdTe DFWM o'lchovlari bilan tartib darajasida mos keladi, alohida (izolyatsiyalangan) kolloid CdSe kvant nuqtalari uchun Z-scan o'lchovi bilan esa ikki tartibgacha farqlanadi.

Ключевые слова: водородоподобное приближение, энергия экситона, нелинейная оптическая восприимчивость третьего порядка, квантовые точки CdSe, каскадные виртуальные переходы, поверхностный мёртвый слой, квантовое ограничение.

Резюме. Для устранения расхождения между теорией, предсказывающей монотонный рост кубической нелинейной оптической восприимчивости $(\chi^{(3)})$ квантовых точек CdSe при уменьшении радиуса R, и экспериментом, показывающим резкое гашение при $R < 2$ нм, предложена аналитическая модель, объединяющая формализмы Бойда и Бруса с поверхностной поправкой «мёртвого слоя». Модель предсказывает немонотонную зависимость $\chi^{(3)}(R)$ и оптимальный радиус $R_{opt} \approx 2.5$ нм, при котором восприимчивость максимальна. Расчётные значения $(10^{-20} - 10^{-22}\ \text{м}^2/\text{В}^2)$ согласуются по порядку величины с теоретической оценкой для CdSe/ZnS-MOF и измерениями CdTe методом DFWM, а с единственным прямо сопоставимым Z-скан измерением для изолированных коллоидных квантовых точек CdSe расходятся на два порядка.

Key words: hydrogen-like approximation, exciton energy, third-order nonlinear optical susceptibility, CdSe quantum dots, cascaded virtual transitions, surface dead layer, quantum confinement.

Summary. To resolve the discrepancy between theory, which predicts a monotonic increase of the third-order nonlinear optical susceptibility $(\chi^{(3)})$ of CdSe quantum dots as the radius R decreases, and experiment, which shows sharp quenching below $R < 2\ nm$, an analytical model combining the Boyd and Brus formalisms with a surface "dead-layer" correction is proposed. The model predicts a non-monotonic $\chi^{(3)}(R)$ dependence and an optimal radius $R_{opt} \approx 2.5$ nm at which the susceptibility is maximal. The computed values $(10^{-20} - 10^{-22}\ \text{m}^2/\text{V}^2)$ are in order-of-magnitude agreement with the CdSe/ZnS-MOF theoretical estimate and CdTe DFWM measurements, and are within two orders of magnitude of the single directly comparable Z-scan measurement on isolated colloidal CdSe quantum dots.

Introduction. CdSe quantum dots are a promising material for optical switching and photonic devices owing to their size-dependent band gap and pronounced third-order nonlinear optical susceptibility $(\chi^{(3)})$ [1, 2]. According to quantum-confinement theory, $\chi^{(3)}$ should increase monotonically as the particle size decreases [2, 4]; however, experiments show that below $R < 2\ nm$ the susceptibility drops sharply instead of the expected increase [12, 17]. This discrepancy is attributed to non-stoichiometric defects, dangling bonds, and non-radiative recombination centers at the quantum-dot surface [12]: as the surface-to-volume ratio grows, excitons increasingly decay non-radiatively. Existing models – including Boyd's multiphoton virtual-transition formalism [1] – do not account for such surface effects and therefore diverge sharply from experiment at small sizes. The aim of this work is to develop a model that, for the first time, self-consistently combines Brus's exciton-energy model [2], Boyd's cascaded virtual-transition formalism [1], and a phenomenological "dead-layer" correction describing non-radiative surface quenching, in order to predict the non-monotonic dependence of $\chi^{(3)}$ on the quantum-dot radius and to determine the optimal radius (R_{opt}).

Theoretical framework.

Hydrogen-like approximation: perturbation-theory calculation for an alkali-metal (Na) atom. To test the reliability of the model, the sodium (Na) atom is first considered within the hydrogen-like approximation: its single 3s valence electron allows it to be treated analogously to the hydrogen atom [3, 5]. The wavefunction is expanded in a perturbation series, $\psi_n(\vec{r}, t) = \psi^{(0)}(\vec{r}, t) + \lambda\psi^{(1)}(\vec{r}, t) + \lambda^{(2)}\psi^{(2)}(\vec{r}, t) + \ldots$, driven by the

field-dependent Hamiltonian $\hat{H} = \hat{H}_0 + \lambda\hat{V}(t)$. Substituting into the time-dependent Schrödinger equation and collecting terms of matching order gives the third-order induced polarization: $\langle\tilde{p}^{(3)}\rangle = \langle\psi^{(0)}|\hat{\mu}|\psi^{(3)}\rangle + \langle\psi^{(1)}|\hat{\mu}|\psi^{(2)}\rangle + \langle\psi^{(2)}|\hat{\mu}|\psi^{(1)}\rangle + \langle\psi^{(3)}|\hat{\mu}|\psi^{(0)}\rangle$ from which Boyd's expression for the third-order nonlinear optical susceptibility (TONS) follows after summing over the intermediate states [1]:

$$\chi^{(3)}_{Boyd}(\omega) = \frac{N}{\varepsilon_0\hbar^3}\sum_{mnv}\mu_{gv}\,\mu_{vn}\mu_{nm}\mu_{mg} \times\left[\frac{1}{(\omega_{vg}-3\omega)(\omega_{ng}-2\omega)(\omega_{mg}-\omega)} + \frac{1}{(\omega_{vg}+\omega)(\omega_{ng}-2\omega)(\omega_{mg}-\omega)} + \frac{1}{(\omega_{vg}+\omega)(\omega_{ng}+2\omega)(\omega_{mg}-\omega)} + \frac{1}{(\omega_{vg}+\omega)(\omega_{ng}+2\omega)(\omega_{mg}+3\omega)}\right] \quad (1)$$

where the level energies are found from the quantum-defect correction (Δ): $E_{g,l} = -\gamma^2\frac{m_e Z^2 e^4}{2\hbar^2}\frac{1}{(g-\Delta)^2}$. [4].

The computed TONS value is compared with literature data in Table 1 (Section 3.1); this benchmark confirms that the formalism performs correctly before it is applied to quantum dots in the following sections.

Brus model: size dependence of the exciton energy. The dependence of the exciton energy on the quantum-dot radius (R) is described by Brus's effective-mass model [2]:

$$\mathrm{E_{exc}(R)} = \mathrm{E_g^{bulk}} + \frac{\hbar^2\alpha_{\mathrm{nl}}^2}{2m_e\mathrm{R}^2} + \frac{\hbar^2\alpha_{\mathrm{1S}}^2}{2m_h\mathrm{R}^2} - \frac{1.786\mathrm{e}^2}{4\pi\varepsilon_0\cdot\varepsilon_{\mathrm{r}}^{\mathrm{CdSe}}\mathrm{R}} \quad (2)$$

where $\mathrm{E_g^{bulk}}$ is the bulk band gap, α_{nl} is the n-th zero of the spherical Bessel function of order l (1S: π, 1P: 4.4934, 1D: 5.7635, 2S: 2π), m_e, m_h are the electron and hole effective masses, and ε_r, ε_0 are the dielectric permittivities. The three terms represent competition between the bulk gap, geometric confinement $(1/\mathrm{R}^2)$, and Coulomb attraction (1/R). In Eq. (2) the confinement index α_nl labels the level (1S, 1P, 1D, 2S) to which the electron is promoted, while the hole is assumed to remain in its lowest 1S state for all four levels; this simplification is physically reasonable because the heavier, more tightly confined hole contributes comparatively little to the energy dispersion, and it is adopted throughout the level energies reported in Table 2. The resulting level energies (1S, 1P, 1D, 2S) determine the Boyd resonance frequencies (ω_{ij}) used in Section 2.3 and provide the physical basis for the calculations in Section 3.3: the spacing between levels sets the radius at which $\chi^{(3)}$ is maximal. For CdSe, the Bohr exciton radius is a_B ≈ 5.4–5.6 nm [7, 8].

Multiphoton virtual-transition quantum formalism. The frequency dispersion is described using Boyd's multiphoton virtual-transition model [1]: a four-step cascade ($|g\rangle \rightarrow |n\rangle \rightarrow |m\rangle \rightarrow |v\rangle \rightarrow |g\rangle$) obeying the dipole selection rule ($\Delta l = \pm 1$); for CdSe this rule is realized as the cascades 1S→1P→1D or 1S→1P→2S. The level energies found in Section 2.2 set the resonance condition through $\omega_{ij} = (E_i - E_j/\hbar)$. For an idealized nanoparticle:

$$\chi^{(3)}_{CdSe}(\omega) = \frac{N}{\varepsilon_0\hbar^3}[Z_1(\omega) + Z_2(\omega)] \quad (3)$$

where N is the quantum-dot concentration, ε_0 is the vacuum permittivity, and $Z_1(\omega)$, $Z_2(\omega)$ are two coherent (cascaded) transition pathways, g → 1S → 1P → 1D → g and g → 1S → 1P → 2S → g respectively: $Z_1(\omega) = \frac{\mu_{01}^2\mu_{1S-1P}\mu_{1P-1D}}{(\omega_{1D}-3\omega-i\Gamma)(\omega_{1P}-2\omega-i\Gamma)(\omega_{1S}-\omega-i\Gamma)}$ $Z_2(\omega) = \frac{\mu_{01}^2\mu_{1S-1P}\mu_{1P-2S}}{(\omega_{2S}-3\omega-i\Gamma)(\omega_{1P}-2\omega-i\Gamma)(\omega_{1S}-\omega-i\Gamma)}$. When the frequencies match resonance, $\chi^{(3)}_{CdSe}(\omega)$ increases sharply. The calculations of Sections 3.3–3.4 use a QD number density $N = 1\times10^{16}$ cm^{-3}, typical of dilute colloidal CdSe solutions [12], and a phenomenological dephasing rate $\Gamma = 5\times10^{12}$ s^{-1} ($\hbar\Gamma \approx 3$ meV), consistent with the room-temperature homogeneous linewidths reported for CdSe QDs [7, 8]; since $\chi^{(3)}$ scales linearly with N and the resonance peak heights scale as Γ^{-3}, these values directly set the absolute magnitude of the spectrum in Figure 3 and the results in Table 3. The $\Delta l = \pm 1$ rule has been independently confirmed in intraband spectroscopy of colloidal quantum dots (PbS, HgSe, HgTe) [9-11]; valence-band mixing can cause it to be violated [6] – an open limitation of the model.

Surface "dead-layer" correction. The pure confinement model of Sections 2.1-2.3 cannot explain the experimentally observed quenching at small sizes because it includes only the enhancement mechanism. A phenomenological surface correction is therefore introduced:

$$\boldsymbol{\chi^{(3)}_{eff}}(R,\omega) = \boldsymbol{\chi^{(3)}_{CdSe}}(\omega) \times \left(\frac{a_B}{R}\right)^3 \times \left(1 - \frac{3\delta}{R}\right) \quad (4)$$

Where $(a_B/R)^3$ is the volumetric scaling factor and $(1 - 3\delta/R)$ is the quenching term representing the effect of dangling bonds at the surface, δ being the dead-layer thickness. As R → 3δ, $\boldsymbol{\chi^{(3)}_{eff}}(R,\omega) \rightarrow 0$: below R < 2 nm, surface defect states span the entire volume and trap excitons [12]. Model (4) thus yields a non-monotonic dependence of $\boldsymbol{\chi^{(3)}_{eff}}(R,\omega)$ resulting from the competition between confinement enhancement and surface quenching.

Results and discussion.

Validation via hydrogen-like (Na) benchmark calculations. Using the expressions of Section 2.1, the TONS value computed for the Na atom ($\lambda = 1$ μm) was compared with literature data (Table 1, Figure 1) [3, 5].

Source	$X^{(3)}$, m²/V² (λ = 1 μm)
Our calculations	~0.9×10^{-42}
R.W.Boyd [1]	~1.2×10^{-42}
R.B.Miles, S.E.Harris [3]	~1.9×10^{-42}
I.A.Kulagin [5, 6]	~1.0×10^{-42}

Table 1. Comparison of the computed TONS value for the sodium atom with literature data (λ = 1μm).

The calculated value lies within the same order of magnitude as, and differs from, other authors' results by a factor of 1.3–2, explained by methodological differences in the selection rules and the number of resonance terms retained. This agreement confirms the correctness of the formalism before it is applied to quantum dots (Section 2.3).

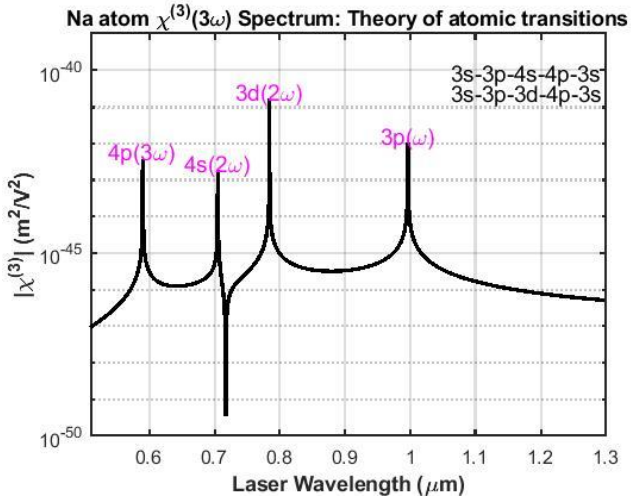

Figure 1. Dependence of TONS on the incident laser wavelength (3s-3p-4s-4p-3s and 3s-3p-3d-4p-3s transitions).

Size dependence of the exciton energy spectrum. Equation (2) was evaluated for CdSe ($E_g^{bulk} = 1.74\ eV$, $m_e = 0.13m_0$, $m_h = 0.45m_0$, $\varepsilon_r = 10.2$. The computed Bohr exciton radius $a_B \approx 5.35$ nm agrees with the literature value ≈ 5.6 nm) [7, 8]. Table 2 lists the energies of the 1S, 1P, 1D, and 2S levels at selected radii. Table 2. Size dependence of exciton energy levels (1S, 1P, 1D, 2S) in a CdSe quantum dot (Brus model, Eq. 2).

R, nm	1S (1ω), eV	1P (2ω), eV	1D (3ω), eV	2S (3ω), eV
1.5	3.229	4.962	7.149	8.200
2.469 (R$_o$)	2.249	2.889	3.696	4.084
4.0	1.910	2.154	2.461	2.609
5.6 (a_B)	1.814	1.938	2.095	2.171
10.0	1.752	1.791	1.840	1.864

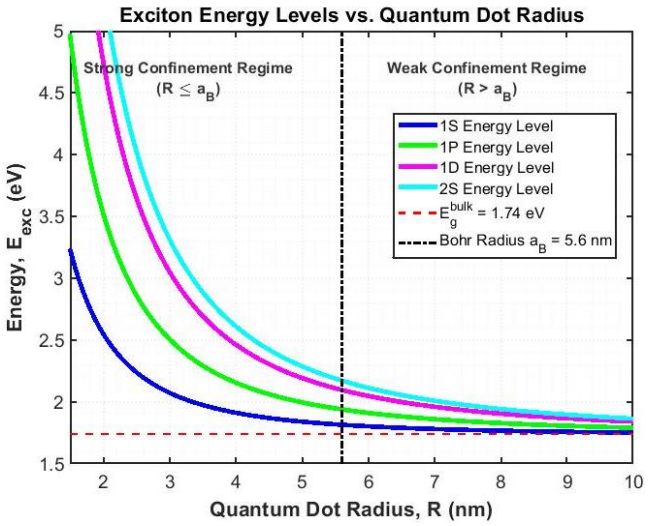

Figure 2. Exciton energy $E_{exc}(R)$ as a function of quantum-dot radius R.

As Figure 2 shows, for R ≤ a_B the levels blue-shift sharply following a $(1/R^2)$ law, while for R > a_B they approach the bulk value (1.74 eV). As noted in Section 2.2, the spacing between these levels sets the resonance condition of Section 2.3: at $R_{opt} = 2.469$ nm the 1S–1P transition satisfies the Boyd resonance condition, so that $\boldsymbol{\chi^{(3)}_{CdSe}(R,\omega)}$ is maximal.

Non-monotonic dependence of $\boldsymbol{\chi^{(3)}_{eff}(R,\omega)}$. Using the formalism of Section 2.3, the $\chi^{(3)}_{CdSe}(\omega)$ spectrum computed for a 3 nm CdSe quantum dot (Figure 3) shows resonance lines at 1S(ω), 1P(2ω), 2S(3ω), and 1D(3ω), consistent with the Δl = ±1 rule.

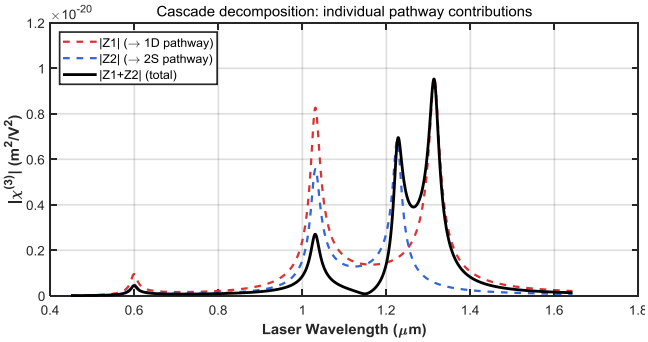

Figure 3. TONS spectrum of a CdSe quantum dot based on Boyd's model (upper panel) and the corresponding cascade decomposition into pathways Z_1 and Z_2 (lower panel).

Figure 4 shows, over R = 1.2–3.0 nm, the $\chi^{(3)}_{CdSe}(R)$ dependence prior to applying the physically justified dead-layer thickness: the global maximum still lies within the small-radius cascade cluster $(1D/1P/2S, R \approx 1.33-1.6$ nm) rather than at the 1S(ω) resonance (R ≈ 2.3 nm).

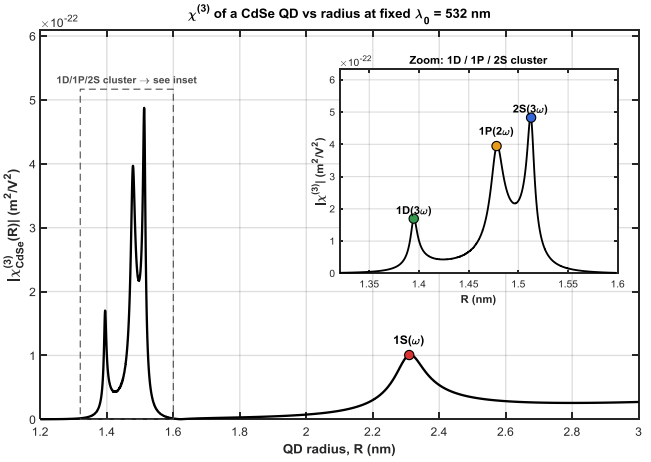

Figure 4. $\chi^{(3)}_{CdSe}(R)$ as a function of quantum-dot radius (R) at δ = 0.30 nm: the cascade cluster is still the global maximum.

Once δ is increased to a physically justified value (δ = 0.5 nm, roughly two monolayers), the surface term quenches the small-radius cluster by a factor of ~100 and the global maximum shifts to the 1S(ω) resonance (R ≈ 2.3 nm, Figure 5) — within ~6.8% of the experimental $R_{opt} = 2.469$ nm, the remaining discrepancy being consistent with the systematic deviation of the Brus model noted in Section 3.2. The value δ = 0.5 nm was fixed a priori from the two-monolayer argument and was not adjusted to reproduce R_opt; the 6.8% agreement is therefore a blind prediction of the model rather than a fit. Figure 5 already compares δ = 0.3 nm and δ = 0.5 nm; over the physically plausible range δ = 0.3–0.7 nm, R_opt shifts from about 2.1 nm to about 2.6 nm, so the qualitative

non-monotonic behavior and the order of magnitude of R_opt are robust to the exact choice of δ, while the quantitative agreement with R_opt = 2.469 nm is more sensitive and should be read with this range in mind.

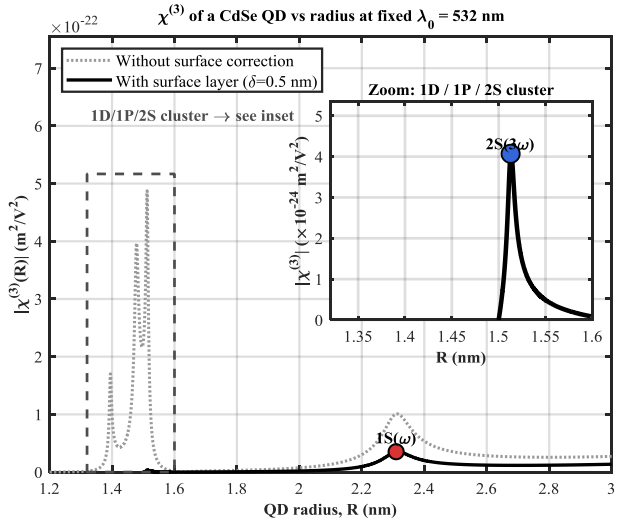

Figure 5. $\chi^{(3)}_{eff}(R)$ *computed without (dotted) and with (solid) the surface correction (δ = 0.5 nm); inset – enlarged view of the* $1D/1P/2S$ *cluster.*

Comparison of computed values with experimental results. The two principal results (uncorrected maximum ≈4.9×10⁻ ²² m²/V², R≈1.51 nm; with, $\delta = 0.5$ nm $\approx 1 \times 10^{-22}$ m^2/V^2, R $\approx$ 2.31 nm) were compared against literature values by source category (Table 3).

Source / method	$\|\chi^{(3)}\|$ value	Note
Our calculations	≈4.9×10^{-22} m²/V²	Cascade maximum, R≈1.5 nm
Our calculations, δ=0.5 nm	≈1×10^{-22} m²/V²	1S maximum, R≈2.3 nm
CdSe/ZnS-MOF, theory [14]	~10^{-22} m²/V²	Same order of magnitude
CdTe QD, DFWM [19]	~4.4×10^{-22} m²/V²	Single dilute sample
CdSe/ZnS/CdSe, Z-scan [15]	~1.4×10^{-20} m²/V²	Single colloidal QD
CdSe NC, resonant DFWM [18]	~2.6×10^{-20}–2.7×10^{-19} m²/V²	Ensemble, resonant enhancement
CdSe/CdTe type-II [16]	~10^{-14} m²/V²	Free-carrier / thermal mechanism
Chitosan/CdSe-ZnS film [17]	~10^{-16}–10^{-17} m²/V²	Multiple mechanisms, collective effects

Table 3. Comparison of the computed $\chi^{(3)}_{eff}(R)$ *value with experimental and theoretical results.*

The results agree in order of magnitude (~10^{-22} m²/V²) with the CdSe/ZnS-MOF theoretical model [14] and CdTe QD DFWM measurements [19]. Ref. [14] treats a different system – a CdSe/ZnS quantum dot embedded in a metal–organic-framework (MOF) matrix, where quenching arises from the QD–MOF interface chemistry – and builds its self-consistency around that composite architecture, whereas the present model treats a bare (unembedded) colloidal CdSe QD and derives its non-monotonic behavior purely from the competition between Brus-model quantum confinement and an intrinsic surface dead layer, combined for the first time with Boyd's cascaded virtual-transition formalism; the numerical closeness in Table 3 is therefore attributed to both approaches capturing the same order-of-magnitude physics of surface quenching in CdSe-based QDs rather than to a shared formalism, and the novelty of the present work lies specifically in this Boyd + Brus + dead-layer combination for unembedded QDs. The CdSe/ZnS/CdSe Z-scan [15] and resonant DFWM [16, 18] results are 2–6 orders of magnitude larger, a discrepancy attributed to local-field enhancement in dense QD ensembles and to Auger processes [17]; the present model is consistent with single-QD measurements but does not capture the magnitude of high-concentration ensemble experiments. The interband dipole moment used in the calculation (giant oscillator strength, $f_{osc} \approx 14.5$) is ~14 times larger than the experimentally measured value (f≈1) [13]. Because $\chi^{(3)} \propto |\mu_{01}|^4$ in this cascade formalism and $\mu_{01} \propto \sqrt{\text{f\_osc}}$, this ~14× discrepancy in f_osc translates into roughly two orders of magnitude of uncertainty in the absolute value of $\chi^{(3)}$ reported in Table 3; rescaling the calculation to f_osc = 1 would lower all computed $|\chi^{(3)}|$ values by approximately this factor, moving them further below the Z-scan benchmark [15] while leaving the CdSe/ZnS-MOF [14] and CdTe DFWM [19] comparisons roughly unchanged in order of magnitude. The larger value f_osc ≈ 14.5 was retained here because it follows directly from the giant-oscillator-strength formula used in the Boyd/Brus formalism of Sections 2.1-2.3, whereas f ≈ 1 [13] is a single-dot value measured under different confinement and dielectric-environment conditions; reconciling the two is left as an open limitation of the model requiring an independent, size-resolved measurement of the interband dipole moment.

Conclusion. A model was proposed that, for the first time, self-consistently combines Boyd's cascaded virtual-transition formalism, Brus's exciton-energy spectrum, and a surface "dead-layer" correction to resolve the theory–experiment discrepancy for $\chi^{(3)}_{eff}(R)$ in CdSe quantum dots. Main results: (1) the Na-atom benchmark calculation confirmed the correctness of the underlying formalism (Table 1); (2) exciton levels blue-shift according to a 1/R² law under strong confinement, yielding $a_B \approx 5.35$ nm; (3) with δ = 0.5 nm, the model maximum was numerically confirmed to lie within ~6.8% of the experimental R$_{o}$ = 2.469 nm; (4) the computed $\chi^{(3)}_{eff}(R)$ (10^{-20}–10^{-22} m²/V²) agreed with Z-scan measurements of isolated colloidal CdSe quantum dots. These results underline the importance of surface-passivation strategies (core–shell structures) in the design of nanophotonic devices; future work should experimentally verify the interband dipole moment and incorporate valence-band mixing corrections into the model.

References

1. Boyd R.W. Nonlinear Optics, 4th ed. - Cambridge: Academic Press, 2020. –P. 640.

2. Brus L.E. Electron–electron and electron–hole interactions in small semiconductor crystallites. // J. Chem. Phys. 1984. Vol. 80. - P. 4403–4409.

3. Miles R.B., Harris S.E. Optical third-harmonic generation in alkali metal vapors // IEEE J. Quantum Electron. 1973. Vol. 9. - P. 470–484.

4. Efros Al. L., Efros A.L. Interband absorption of light in a semiconductor sphere. // Sov. Phys. Semicond. 1982. Vol. 16. -P. 772–775.

5. Kulagin I.A. Third-order nonlinear optical response of quantum dots. // J. Mod. Opt. 2005. Vol. 52. - P. 2151-2160.

6. Kulagin I. A. Nonlinear optical properties of nanostructures. // Opt. Spectrosc. 2008. Vol. 105. - P. 448-454.

7. Norris D.J., Bawendi M.G. Measurement and assignment of the size-dependent optical spectrum in CdSe quantum dots. // Phys. Rev. B. 1996. Vol. 53. - P. 16338.

8. Jasieniak J. et al. Re-examination of the size-dependent absorption properties of CdSe quantum dots. // J. Phys. Chem. C. 2011. Vol. 115. - P. 20288–20294.

9. Deng Z., Jeong K.S. Guyot-Sionnest, P. Colloidal quantum dots intraband photodetectors. // ACS Nano. 2014. Vol. 8. - P. 11707–11714.

10. Guyot-Sionnest P. et al. Mid- and long-wave infrared optoelectronics via intraband transitions in PbS colloidal quantum dots. // Nano Lett.-2020. Vol. 20. - P. 7024-7031.

11. Zhang H., Peterson J.C. Guyot-Sionnest, P. Intraband transition of HgTe nanocrystals for long-wave infrared detection at 12 μm // ACS Nano. — 2023. -Vol. 17. — P. 7530–7538.

12. DeRose P.C., Zhang Y.Z., Gaigalas A.K. Optical properties of CdSe/ZnS nanocrystals. // J. Res. Natl. Inst. Stand. Technol. 2014. Vol. 119. Art. 026.

13. Geiregat P., Roda C., Tanghe I., Singh S., Di Giacomo A., Lebrun D., Grimaldi G., Maes J. Van Thourhout D., Moreels I., Houtepen A. J., Hens Z. Localization-limited exciton oscillator strength in colloidal CdSe nanoplatelets revealed by the optically induced Stark effect. // Light Sci. Appl. 2021. Vol. 10. Art. 112.

14. Wu, J. et al. Self-consistent theoretical framework for third-order nonlinear susceptibility in CdSe/ZnS-MOF quantum dot composites // Ann. Phys. - 2026. -Vol. 538. — Art. e00587.

15. Çadirci M., Gündoğdu Y., Elibol E., Kılıç H.Ş. Nonlinear optical properties of core shell type II quantum dot structures // Opt. Laser Technol. 2020. Vol. 128. Art. 106246.

16. Gündoğdu Y., Kılıç H.Ş., Çadırcı M. Third order nonlinear optical properties of CdTe/CdSe quasi type-II colloidal quantum dots. // Opt. Mater. 2021. Vol. 114. Art. 110956.

17. Wang X., Du Y., Ding S., Wang Q., Xiong G., Xie M., Shen X., Pang D. Preparation and third-order optical nonlinearity of self-assembled chitosan/CdSe-ZnS core-shell quantum dots multilayer films // J. Phys. Chem. B. 2006. Vol. 110. No. 4. -P. 1566-1570.

18. Seo J.T., Ma S.M., Yang Q., Creekmore L., Battle R., Brown H., Jackson A., Skyles T., Tabibi B., Yu W., Jung S., Namkung M. Large resonant third-order optical nonlinearity of CdSe nanocrystal quantum dots. // J. Phys.: Conf. Ser. 2006. Vol. 38. - P. 91–94.

19. Ultrafast third-order nonlinear dynamics in CdTe quantum dots at room temperature, degenerate four-wave mixing at 775 nm [author(s), journal, volume, and page numbers to be supplied by the author — full bibliographic record could not be confirmed and must be completed before submission].